PERGAMON

International Journal of Heat and Mass Transfer 45 (2002) 4479–4491

International Journal of HEAT and MASS TRANSFER

www.elsevier.com/locate/ijhmt

An experimental investigation into the heat transfer on wing walls in a circulating fluidized bed boiler

Animesh Dutta, Prabir Basu *

Department of Mechanical Engineering, Dalhousie University, Halifax, P.O. Box 1000, Nova Scotia, Canada B3J 2X4

Received 28 November 2001; received in revised form 11 April 2002

Abstract

Experiments on wing wall were carried out in a circulating fluidized bed pilot plant of 1000 mm × 500 mm in cross section and 5000 mm in height operated at room temperature. A wing wall (918 mm × 500 mm) was hung at two different positions in the riser. A downward solids flow was noticed when the wing wall was located at the top of the riser, but no downward solids flow was observed on its surface when the wing wall is placed 1300 mm below the roof. For a given operating condition, the heat transfer coefficient on the wing wall was higher when it was placed at the top of the riser than when located at mid-height. The difference in heat transfer between water wall and wing wall, as observed in the present experiment, is similar to that noted in commercial boilers.

1. Introduction

Wing walls or platen tube panels are important parts of a circulating fluidized bed (CFB) boiler. These heating surfaces extract the additional amount of heat the boiler furnace needs to lose to maintain a furnace exit gas temperature of 800–850 °C. A wing wall can be either a part of the evaporator or superheater of the boiler. Typically wing walls hang from the roof (Fig. 1) and extend from the front wall to some distance towards the opposite wall, where the furnace exit is located. The CFB boilers often use more than one wing wall to absorb the required amount of heat, which could be as high as 30% of that absorbed by the furnace walls.

A great deal of information [1–4] is available on heat transfer on enclosing walls of the furnace which are commonly know as water walls. A large body of data on heat transfer coefficients for the furnace walls in both laboratory and commercial units are also available [1,4]. As far as is known, no information on heat transfer or hydrodynamics on wing wall is available in published literature. Wing walls, which are located away from the walls, may operate under hydrodynamic conditions different from those on the walls. Therefore, it is not known if the experimental data on water wall or the mechanistic model [5] for the water wall can be applied directly to wing walls.

The present work is probably the first attempt in open literature to report information on wing walls. It provides preliminary data on heat transfer in wing walls measured in a large pilot plant operated at room temperature and compares measured data with those on vertical riser walls.

2. Experiment on pilot plant

2.1. Description of pilot plant

Experiments on the wing walls and the enclosing water wall were carried out using a closed loop cold-model CFB riser of 1000 mm × 500 mm rectangular cross-section. The system, illustrated in Fig. 1 consists of a riser, two separators, two standpipes for storing recirculating solids and a J-valve to feed solids back into the riser. The riser is 5000 mm in height. Clear plastic (LEXAN) was used on the front wall along the height of

* Corresponding author. Tel.: +1-902-494-3227; fax: +1-902-429-4867.

E-mail address: prabir.basu@dal.ca (P. Basu).

0017-9310/02/$ - see front matter
PII: S0017-9310(02)00148-5

Nomenclature

A	projected area, m^2
G	external solid mass flux, $kg\,m^{-2}\,s^{-1}$
h	heat transfer coefficient, $W\,m^{-2}\,K^{-1}$
H	height from the bottom of the heating strip of the wing wall, m
P	power input, W
$\dot{Q}$	heat flux, $W\,m^{-2}$
T	temperature, K
V	velocity, $m\,s^{-1}$

Subscripts

b	bed
s	superficial
w	wall
x	local

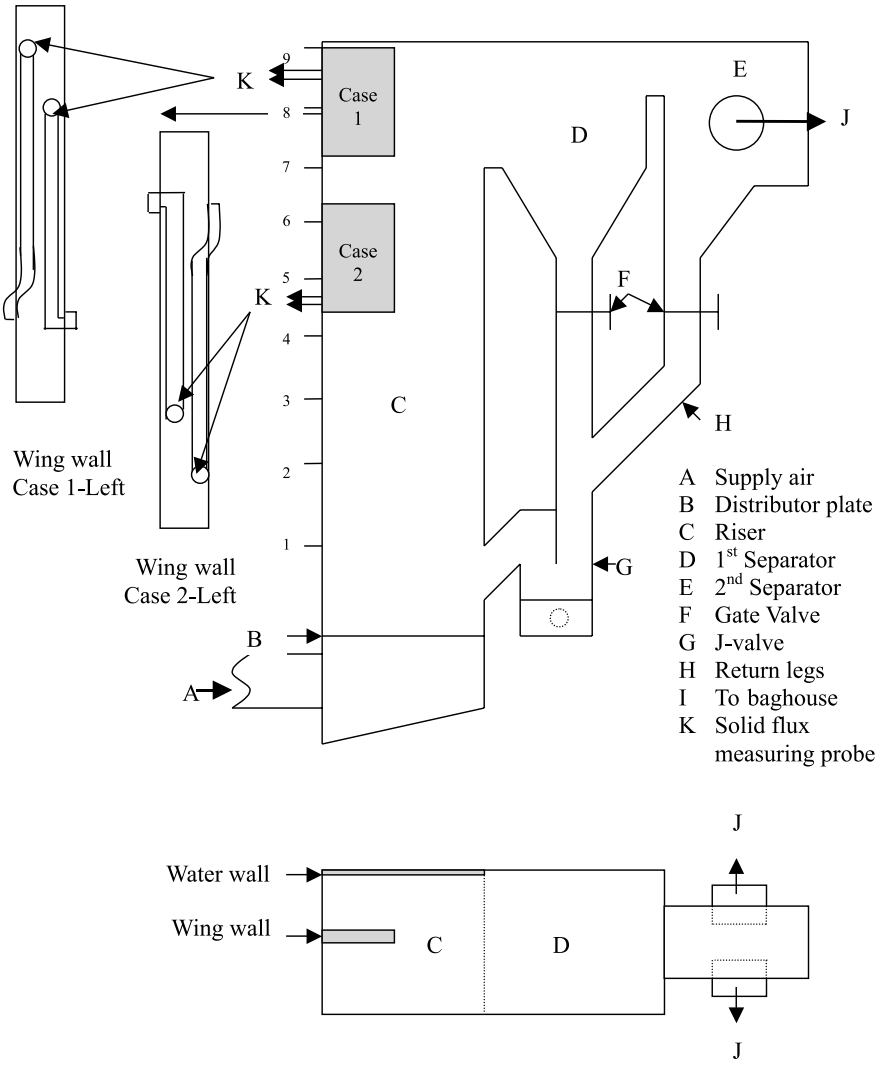

Fig. 1. Schematic diagram of the experimental unit.

the riser column for visual observation whereas the other three walls were made of wood lined with an aluminum sheet. The aluminum sheets were used to ensure a smooth surface, because roughness might affect the hydrodynamics within the riser. Pressure taps are located on the side wall of the riser column at 500 mm

intervals (Table 1). Air was provided by a 2.5 m^3/s, 11.2 kPa fan. Air enters the bottom of the riser through a multi-orifice (9 mm diameter) distributor of 20% opening area coupled with a fine wire mesh of 50% opening area. The superficial gas velocity was measured by both venturi meter and pitot tube arrangements. The highest superficial velocity in the experiments was 5 m/s.

At the top of the column, entrained solids were carried by the gas from the riser to the separators as shown in Fig. 1. Air leaving the secondary separator was led to the baghouse and then to the suction of the fan. Solids in the standpipe entered the riser from the J-valve through a 140 mm ID clear plastic (Acrylic) tube centered 700 mm above the distributor. The wing walls were hung at two positions marked as Case 1 and Case 2 as shown in Fig. 1.

2.2. Wing wall

The wing wall was 918 mm long, 500 mm wide and 50 mm thick. It had heaters placed on it in several locations as shown in Fig. 2. It was hung in the upper part of the fluidized bed riser at 1300 mm in (Case 2) and at 50 mm in (Case 1) below the roof of the riser (Fig. 1). The movement of the wing wall was restricted by holding it to the side wall with long wooden screws and coupling it with an extension rod from the front wall of the riser at its right bottom corner. This ensured a rigid and stable support when it was suspended in the riser.

The wing wall was fabricated of 6.25 mm thick low conductivity Tivar 1000 antistatic UHMW polyethylene. It was made of two sheets of this material, one on each side of the wing wall supported by 37.5 mm strips of the same material along the edge. Fiberglass insulated flexible silicon rubber heaters of low thermal conductivity, were attached to each side of the wing wall. The heaters (2 nos 610 mm $\times$ 50 mm and 6 nos 50 mm $\times$ 152 mm) were installed on both sides of the wing wall (Fig. 2) to reduce heat loss from the walls. The heaters were placed in grooves on both surfaces, in such a way that they were flush with the surfaces. Double sided insulating fiberglass tape was applied between the heaters and the surfaces within these grooves. These heaters are thermally insulated by fiberglass on all four sides.

The heaters were chosen because they are very thin (0.7 mm) and are made of a material with a low thermal conductivity. Such heaters are known to have [6] a constant heat flux. All the heaters were electrically connected in parallel with each other. The temperature distribution over the heated surface was measured from the outer side by 22 thermocouples. In the present study, Teflon coated T-Type thermocouples (0.3 mm thick) were attached to the heaters. These thermocouples have a resolution of 0.1 °C and a response time of 0.3 s. Details of the thermocouples and their locations are shown in Fig. 2. Two additional thermocouples were used to measure the gas–solid suspension temperature. Connecting leads for the thermocouples and the heaters were routed internally through the interior of the wing wall. This was done to keep the surface of the wing wall smooth. All wires were collected in one corner of the wing wall. From there they ran first through the side of the wing wall and then through the sidewall of the fluidized bed riser. The heaters were connected with the power source through a wattmeter and an auto transformer (variac). The heat flux of the heaters was controlled by the variac.

2.3. Solids flux measuring system

A non-isokinetic probe was used on each side of the wing wall to measure the upward and downward solids flux. They were located 310 mm from the sidewall of the riser and 1500 and 720 mm below from the top of the roof for Case 2 and Case 1 respectively. Details are given in Table 1 and Figs. 1–3. As per the suggestion of Rhodes et al. [7], the suction air velocity inside the probe was maintained within the range of 4–7 m/s. The probes were 7.5 mm inside diameter, with one opening on the outside of the wing wall, and the other opening within the wing wall. The opening on the inside was attached to flexible plastic tube. This tube first ran through the side of the wing wall and then through the side of the fluidized bed. Valves were attached to the end of each tube to control the flow of solids.

2.4. Water wall

A heating strip, 610 mm long and 50 mm wide, was attached to one side of the riser wall, 1500 mm below from the roof of the riser. This heating surface simulated the enclosing water wall. It was used to compare the heat transfer coefficient of the water wall with that on the wing wall (Case 2) at a specific height. The water wall test section was similar to the wing wall section except that it was flush with the sidewall of the riser instead of hanging from the roof. Details are on Fig. 4.

2.5. Experimental techniques

To conduct the experiments, the wing walls were placed in two positions, referred to here as Case 1 and Case 2 (Fig. 1). The test section, simulating the water wall, was kept on the sidewall of the riser at 1500 mm below the roof. The heat transfer coefficient was measured after a steady-state condition was reached. The gas–solid suspension was first allowed to flow over the heat transfer surface at a given velocity and then the power for the heater was switched on. Once the temperature of the surface reached a steady value, the local heat transfer coefficient between walls and the bed was determined from the flowing equation

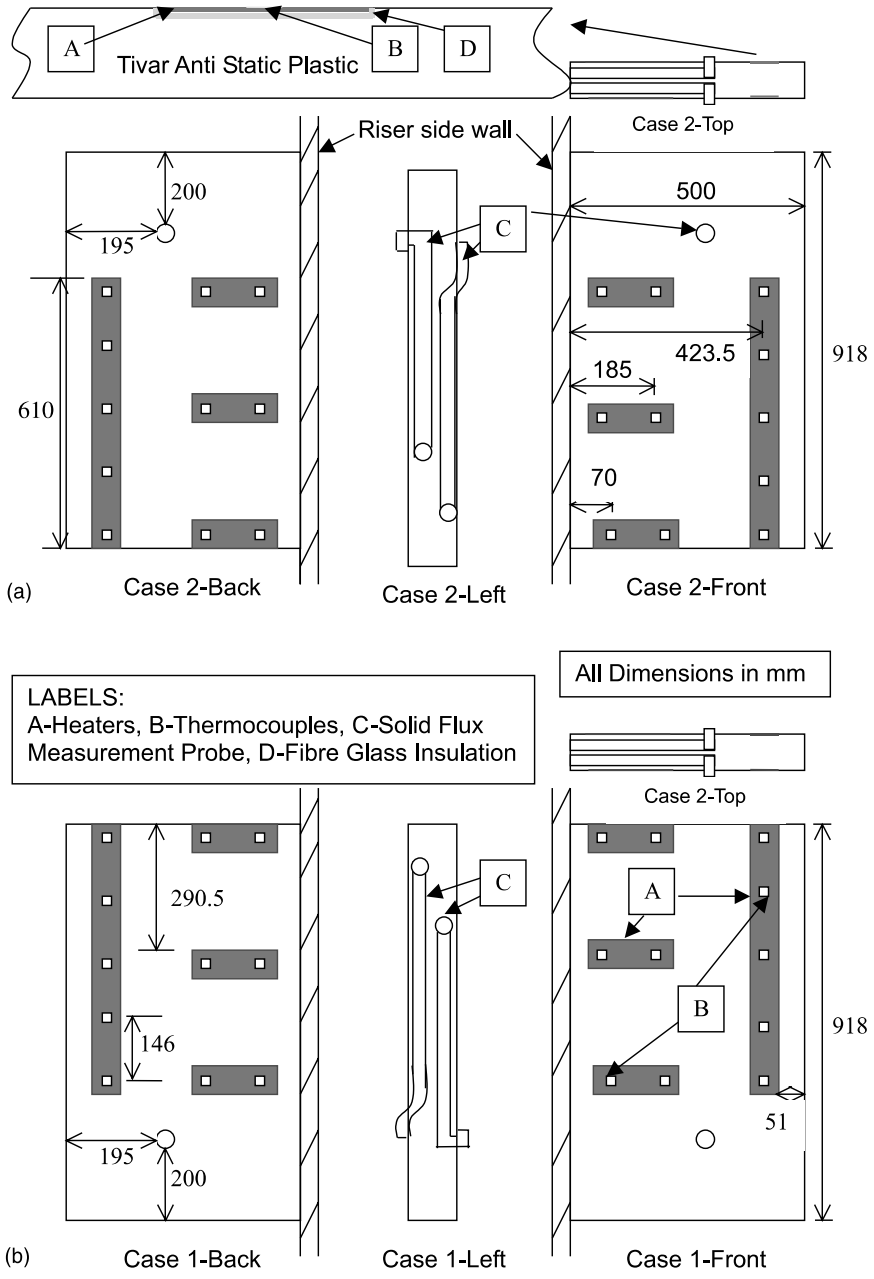

Fig. 2. Details of experimental setup of wing wall: (a) wing wall placed at 1300 mm below the roof (Case 2) and (b) wing wall placed at the top of the roof (Case 1).

$$h_x = \frac{\dot{Q}}{(T_{wx} - T_b)} \tag{1}$$

The heat flux $\dot{Q}$ is calculated by dividing the power input, P, by the heater area, A.

The input power, P, can be calculated by two different ways:

(a) by measuring the voltage across the autotransformer and the current by ammeter,
(b) by reading values directly off the wattmeter.

Both methods gave similar results in all experiments. Therefore, the simpler method described in (b) was used to estimate the heat flux of the heating surface.

Table 1
Locations of pressure transducers in the riser

Transducer no.	Height, to midpoint of measurement section from distributor (m)
(a) Differential pressure transducers	
1	0.8
2	1.5
3	2
4	2.5
5	3
6	3.5
7	4
8	4.5
9	5
(b) Absolute pressure transducers	
At bottom	0.06 m
(c) Solid flux measuring probe	
	At the surface of the wing wall
Case 1	
From roof	720 mm
From side wall	310 mm
Case 2	
From roof	1500 mm
From side wall	310 mm

In the setup for solids flux measurements, solids were collected through the trap over a specified period of time. The probe was purged by a three way valves until sampling started. It also allowed the suction rate to be set before the start of the sampling period (Fig. 3). The solids flux rate was obtained by weighing the particles collected over a specified period of time. The net downward solids flux was obtained by subtracting the upward solid flux from the downward solids flux and vise versa. The probe was calibrated by integrating the flux profile over the cross sectional area of the riser and compared that with the externally measured solids flux.

The superficial velocity was measured in the riser using the venturimeter installed in the air duct. The solids circulation rate was measured by means of two knife valves in the upper part of the return legs, located just below the two separators. The solids circulation rate was calculated by measuring the time for a known volume of solids to accumulate on top of the knife valve after the valve was closed.

For each experiment, the solids valve was opened allowing solids to flow into the riser. When the solid levels in both return legs remained unchanged the system was deemed to have reached a steady state condition.

2.6. Bed material

Nova Scotia sand having a mean diameter 263 μm, particle density of 2564 kg/m^3 and bulk density of 1320 kg/m^3 was used as the bed material. The particle size distribution is given in Table 2.

3. Results and discussion of data from CFB pilot plant

3.1. Hydrodynamics

The wing wall setup was hung from the top of the riser at two different locations;

1. middle of the left wall and at the top of the riser.
2. middle of the left wall and 1.3 m below from the top of riser.

3.1.1. Case 1 (top of the riser)

In Case 1, a net downward solid flow was noticed on the surface of the wing wall as shown in Fig. 5. Data,

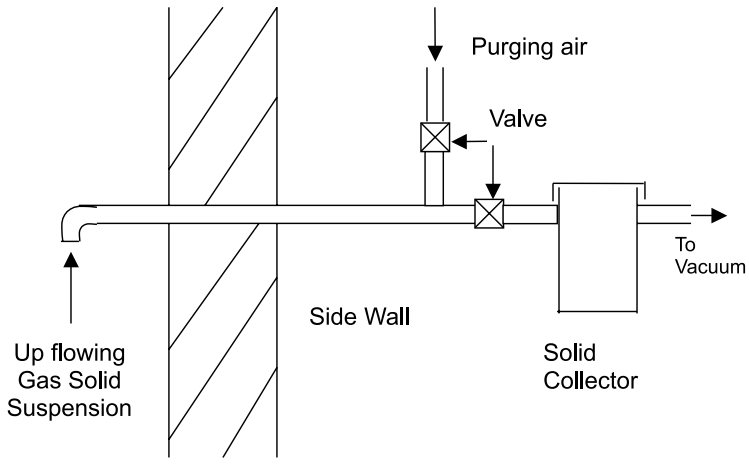

Fig. 3. Schematic diagram of solid flux measuring probe.

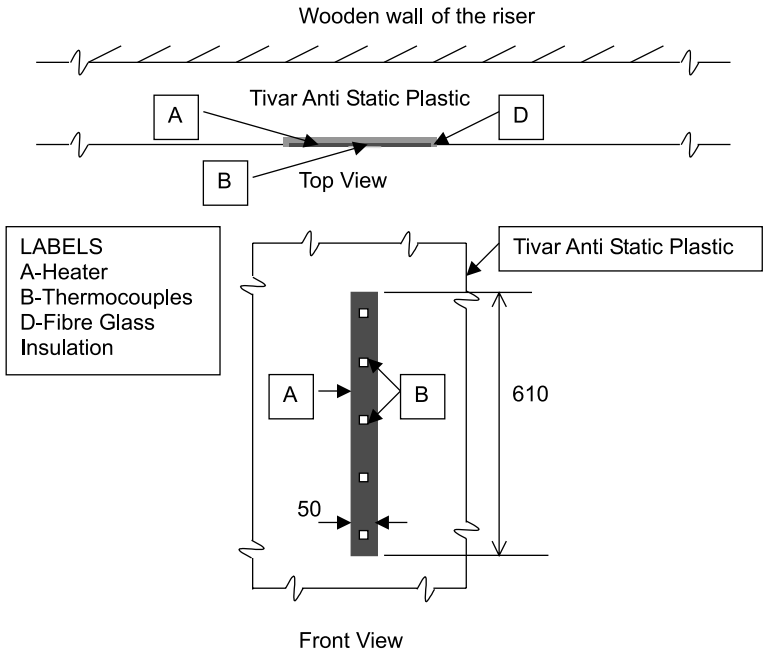

Fig. 4. Details of experimental setup of water wall.

Table 2
Size analysis of "00" grade Nova Scotia sand used in the experiments

Diameter range (μm)	Sample weight (g)	Weight fraction, x_i	$d_{p,i}$ (mm)	$x_i/d_{p,i}$ (mm^{-1})
600–500	15	0.05	0.550	0.092
500–425	39	0.13	0.4625	0.285
425–335	86	0.29	0.380	0.765
335–250	55	0.19	0.2925	0.635
250–212	37	0.13	0.231	0.541
212–180	25	0.08	0.196	0.431
180–150	19	0.06	0.165	0.389
150–125	10	0.03	0.1375	0.246
125–106	7	0.02	0.1155	0.205
106–0	3	0.01	0.053	0.191
	$\sum = 296$			$\sum(x_i/d_{p,i}) = 3.8$ $d_p = 263$ μm

collected by the solids measuring probe, show that the net downward flux of solids increased with an increase in the external solid circulation. This observation can be explained as follows. The upward moving gas turns 90° at the top of the riser to move towards the riser exit. So, a stagnant zone or cavity is created at the top corner of the riser just opposite to the exit to the cyclone. Though there could be much eddies, the net upward gas velocity is zero in that area. The streamlines of gas carrying solids in this region was clearly visible through the transparent front wall. The test zone was observed to lie above of this gas flow path. On the other hand, because of their higher momentum, the solids continued to move upwards. Some of them directly hit the roof of the riser while others gradually lost their momentum due to inertial effect and fell down in the cavity. The ratio of downward and upward fluxes gives the relative measure of downward solid flux. It was 1.6 while the external solid recycle rate was 2.0 kg/m^2 s. This ratio increased to 2.2 when external recycle rate was increased to 8 kg/m^2 s. This suggests a relatively mild influence of the recycle rate.

3.1.2. Case 2 (1300 mm below the roof)

In this case, the solid flux was measured further down the riser, but still away from the wall. Unlike the

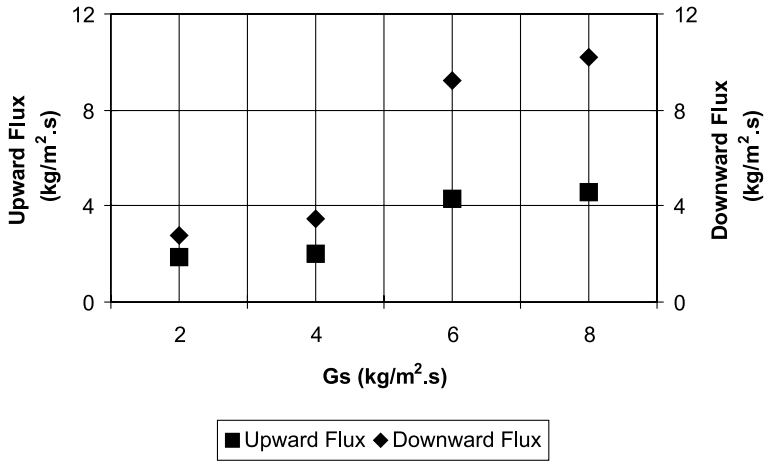

Fig. 5. Variation of upward and downward solids mass fluxes with external solids circulation rates for a constant superficial velocity ($V_s = 3.9$ m/s) for wing wall (Case 1).

previous case, no net downward solids were noticed on the surface of the wing wall in this case (Fig. 6a and b). This observation can be explained by the core annulus structure, the widely accepted hydrodynamic model for the CFB riser. According to this model, the solid concentration is very low at the center of a CFB riser and it increases exponentially towards the wall of the riser [8]. As the wing wall in the present experiment was located at the middle of the riser, one can expect a very low concentration of solid in that region. Glicksman [9] reported that the gas velocity at the center of a CFB riser is as much as twice of the cross sectional average gas velocity (superficial velocity). Neither high upward gas velocity nor low concentration of solid favor formation of clusters, which flow downward on the wing wall. The presence of solids reduce the thickness of the boundary layer on the wall giving a flatter velocity profile in the radial directions compared to when gas alone is flowing [10–12]. For this reason, solids near the wing wall at the center do not flow downward. However, when the solid concentration is increased greater number and heavier clusters are formed. Consequently, solids tend to flow down more on the wing wall. Measured data showed (Fig. 6a and b) that the net upward flux of solids on the surface decreases with the increasing of external solid circulation. This was irrespective of superficial velocity.

3.2. Heat transfer

To study the effect of varying hydrodynamic conditions on the heat transfer, local heat transfer coefficients

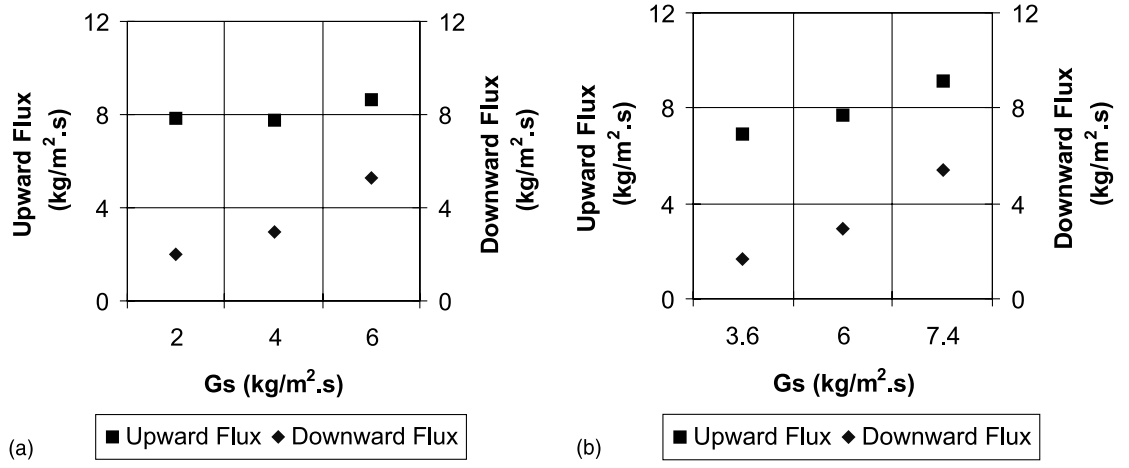

Fig. 6. Variation of upward and downward solids mass fluxes with external solids circulation rates at two different superficial velocities ($V_s = 3.9$ m/s, $V_s = 4.4$ m/s) for wing wall (Case 2).

were measured on the wing wall at both upper and lower locations. Experiments were carried out at different external circulation rates and superficial velocities. A typical data on local wall temperature, average bed temperature and heat flux are shown in Table 3. The temperatures on both side of the wall were found similar and local wall temperatures were estimated by averaging the recorded values from both sides. Results shown in Figs. 7–9 compare the results for both cases, the variation of heat transfer coefficients along the height of the wing wall at a fixed operating condition. For Case 1, (Fig. 7), at higher external circulation rates (8 and 6 kg/m^2 s) the heat transfer coefficient decreased gradually from the top of the heating strips towards its bottom. This can be explained by the observed net downward solids flow (Fig. 5) along the height of the wing wall. The net downward solid flux was in excess of 4 kg/m^2 s. As the layer of particles sweeps down the heating strip, it gradually approaches thermal equilibrium with the surface. This reduces the thermal driving force which is the temperature differential across the gas film. This causes lower heat transfer and consequently lower heat transfer coefficient which is based on temperature difference between the wall and the average bed temperature. These results support the hydrodynamic behavior in the riser as observed by the solid flux measurement probe. Similar observations are also made on heat transfer to the water wall [13,14]. These results showed higher heat transfer coefficients at higher external solid circulation rates.

Table 3
Typical data on local wall temperature, average bed temperature[a] and heat flux[b]

Distance along the heating strip (mm)	12.7	158.7	304.8	450.8	596.8
Local wall temperature, T_{wx}	51	55.6	57.4	56.9	57.8
Calculated local heat transfer coefficient, h_x	86.7	56.3	49.5	51.2	48.2

[a] Average bed temperature, $T_b = 42.5$.
[b] Heat flux = 736.9 W/m^2.

However, at a lower external solids circulation rate (2–4 kg/m^2 s), the heat transfer coefficient on the lowest point of the wing wall is higher than that on the point just above it. The heat transfer in cold bed comprises contributions of both gas convection and particle conduction. In the case of low external circulation rate, we can see from Fig. 5 that both upward and downward solid fluxes are very low. This gives a low particle concentration in the upper bed. Thus, here the gas convection from the upward gas flow is more dominant than the conduction from the moving particles. In case of forced convection on a flat plate, the heat transfer on the leading edge is highest. Thus in the present case, the heat transfer at the bottom of the wall is highest. To verify this hypothesis, several tests were carried out without any solids in the riser. Results clearly show that for pure gas convective the heat transfer coefficient is highest at the lowest point of the wing wall.

Results from Case 2 where the wing wall was at 1300 mm below the top of the roof (Fig. 8) showed a different scenario. The heat transfer coefficient is higher at the

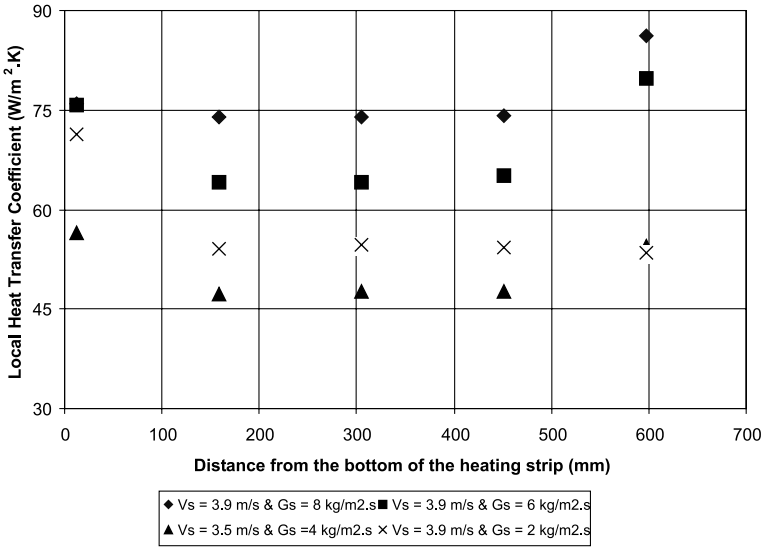

Fig. 7. Local heat transfer coefficients measured along the height of the wing wall placed at the top of the roof at different operating conditions (Case 1).

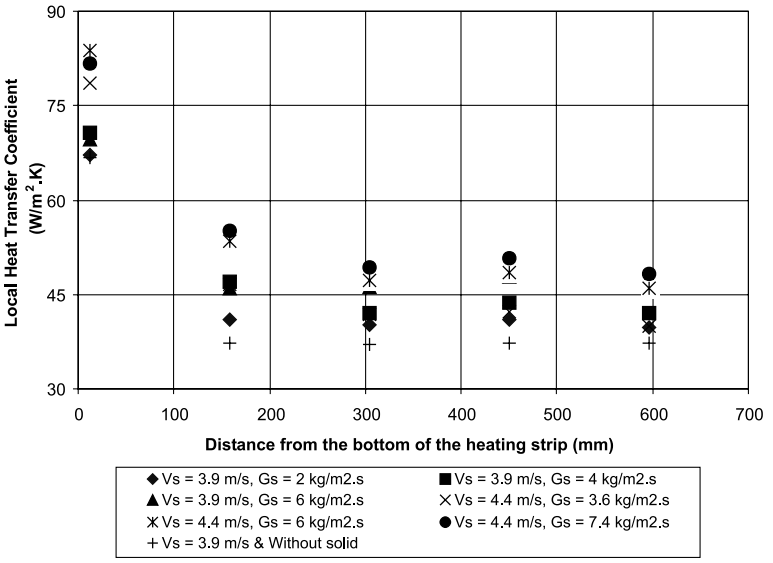

Fig. 8. Local heat transfer coefficients measured along the height of the wing wall placed 1300 mm below the top of the roof at different operating conditions (Case 2).

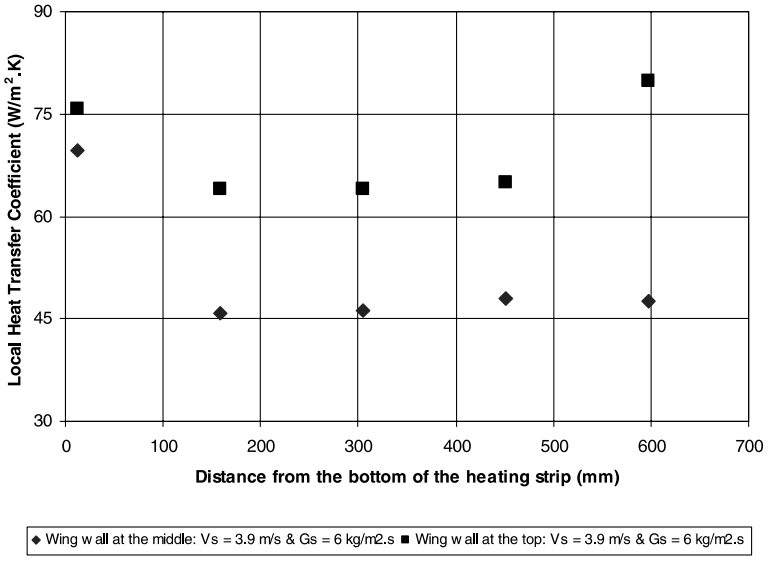

Fig. 9. Comparison on local heat transfer coefficients along the height of the heating strip between Case 1 and Case 2 for a specific operating condition.

bottom of the heating strip at all external solids circulation rates. The heat transfer coefficient gradually decreases down to the heating strip. It is apparent that there is no net downward solids flow along the wing wall at this position. Solids flux measurements (Fig. 6) supported the findings. In general, heat transfer coefficient increases with increasing superficial velocity and external solids circulation rates. The difference in heat transfer coefficients between two superficial gas velocities (3.9 and 4.4 m/s) at a fixed circulation rate of 6 kg/m^2 s is significant at the lowest point of the wing wall. The heat transfer at the lowest position depends mainly on the gas velocity. At higher velocity, the Reynolds number is higher and the convective heat transfer coefficient will also be higher in this region of developing thermal boundary layer. However, further up in the developed region, due to the formation of the thermal boundary layer, heat transfer coefficient is low and is nearly

constant. The contribution of particle convection is also important here because of high net upward solid flux. As the solid flux is upwards, the particle convection is also higher in the lower end. For the same reason the particle convection decreases towards the top. Owing to the particle convection, the heat transfer coefficient in this case is higher than the heat transfer coefficient measured (Fig. 8) without solid.

The relative importance of downward solids flow, along the heating strips for a given velocity and circulation rates is shown in Fig. 9. In Case 1, at the highest point of the heating strip, the heat transfer coefficient is nearly 1.5 times the value recorded in the highest point of the wing wall in Case 2. However, at the lowest point where gas convection is dominant both have the very similar heat transfer coefficients. The upper wing wall

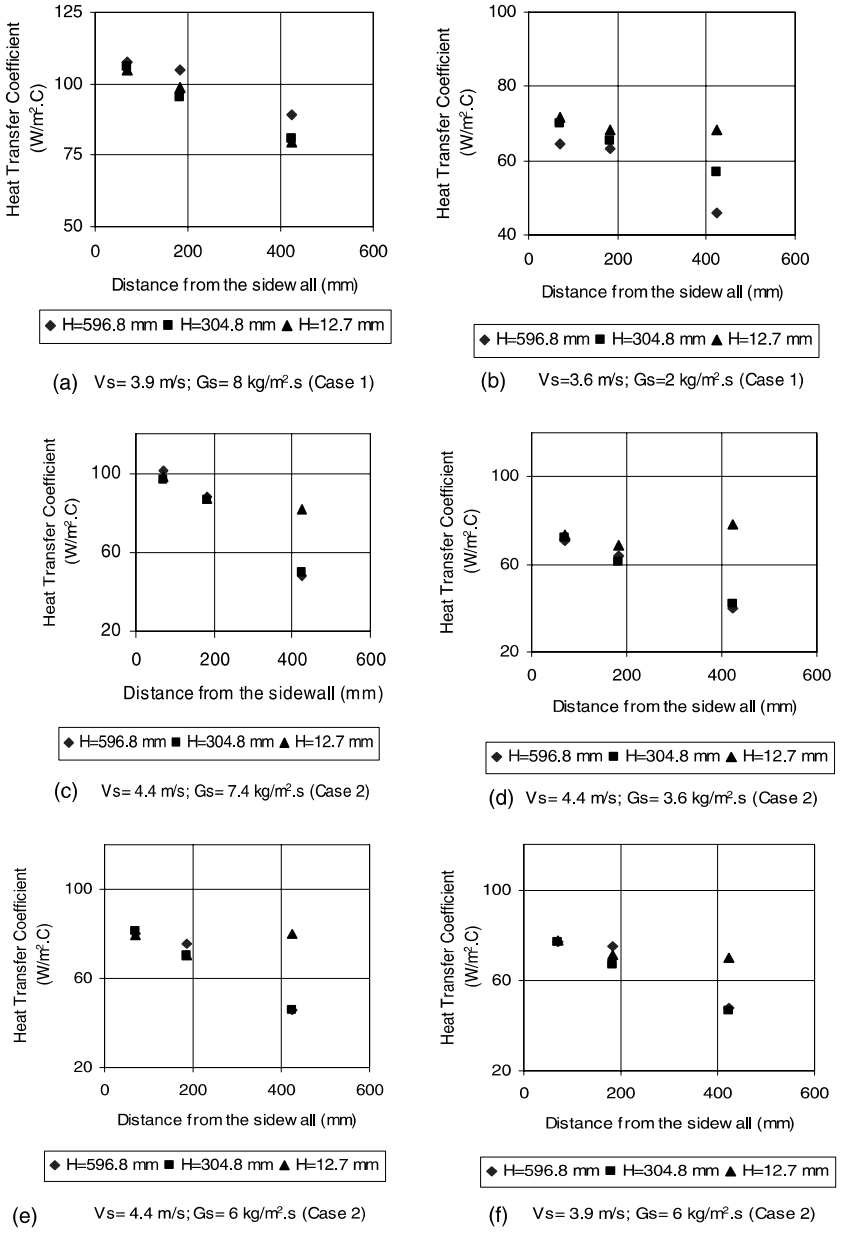

Fig. 10. Local heat transfer coefficients along the width of the wing wall for both Case 1 and Case 2: (a) $V_s = 3.9$ m/s; $G_s = 8$ kg /m^2 s (Case 1), (b) $V_s = 3.6$ m/s; $G_s = 2$ kg/m^2 s (Case 1), (c) $V_s = 4.4$ m/s; $G_s = 7.4$ kg/m^2 s (Case 2), (d) $V_s = 4.4$ m/s; $G_s = 3.6$ kg/m^2 s (Case 2), (e) $V_s = 4.4$ m/s; $G_s = 6$ kg/m^2 s (Case 2) and (f) $V_s = 3.9$ m/s; $G_s = 6$ kg/m^2 s (Case 2).

(Case 1) shows higher heat transfer in the upper end of the heating surface because here the downward solids flux is higher than that at the top of the lower wing wall (Case 2). However, as one moves down, the downward flux declines because the solids sweep upward over the upper wing wall due to higher local gas velocities at those positions. Therefore, the difference of heat transfer coefficients on the lower end of wing walls at two locations is low. Finally, the lowest point of the wing walls is influenced by the strong entry effect of upward moving gas and solids. Thus both have higher but similar heat transfer coefficients.

The local heat transfer coefficient along the width of the wing wall is shown in Fig. 10. Local heat transfer coefficient is plotted for different operating conditions at three different heights measured from the bottom of the heating strip and along the width (distance measured from the sidewall) of the wing wall. Near the wall the heat transfer coefficient is higher suggesting a greater solid concentration at the wall and on the corner.

As the external solid circulation increases, the heat transfer coefficient also increases due to the increase of suspension density as well as solids concentration. In Case 1 (upper location), an interesting observation is made when the CFB unit was operating for two different external solids circulation rates (Fig. 10a and b). At the top of the heating strip ($H = 596.8$ mm), the heat transfer coefficient was higher than that at the bottom. This is due to a greater downward solids flow at higher circulation rates. On the other hand, at lower circulation rate the heat transfer coefficient at the bottom ($H = 12.7$ mm) is higher than that at the top signifying an upward solid flow. A wide variation is observed at the position 423 mm from the sidewall of the riser. This is because the heating strip is a long (610 mm in height) one instead of short (50 mm in height) one, which forms thermal boundary layer on the heating surface along the height of the strip.

Within the range of operating parameters ($V = 3.5$–4.4 m/s and $G_s = 2$–7.4 kg/m^2 s) a net upward flux (Fig. 6a and b) was always observed in Case 2 (Fig. 10c–f). The hydrodynamic observation also supports the heat transfer measurements. Taken at specific points, for example, Fig. 10c–e show that the local heat transfer coefficient near the corner (70 and 185 mm away from the side wall of the riser) increases with the external solid circulation rates. However, no noticeable change was observed for the position 423.5 mm away from the sidewall. However, in Fig. 10e and f, due to the different superficial velocity, there was a noticeable change on that position. This is explained by the followings. At the corner solid concentration is higher [15]. Therefore, the local heat transfer coefficient here depends more on the solid concentration than on the gas convection. The gas convection is more predominant in the middle of the riser. It is also seen that smaller the heating surface area, the larger the heat transfer coefficient. This supports the observations made by other researchers elsewhere [16].

3.3. Comparison between water wall and wing wall heat transfer

Local heat transfer coefficients along the water wall were obtained for different superficial velocities and external solids circulation rates. The variations are plotted in Fig. 11 where the distance along the water wall is measured from its bottom to the top. Similar to the trend reported earlier [13,14], the local heat transfer

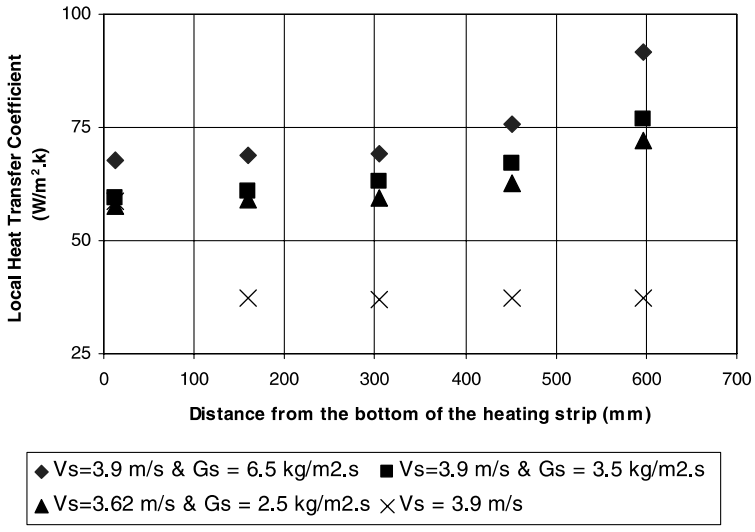

Fig. 11. Local heat transfer coefficients measured along the height of the water wall at different operating conditions.

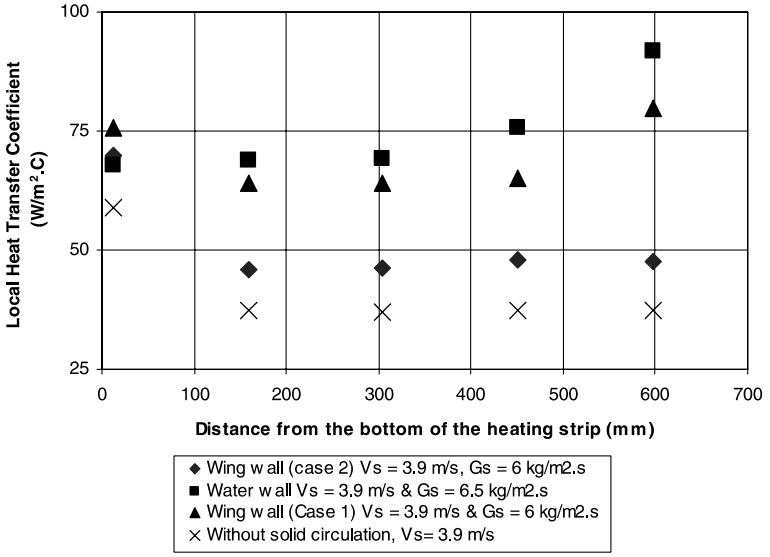

Fig. 12. Comparison on local heat transfer coefficients along the height of the heating strips for wing wall (Case 1 and Case 2) and water wall at a specific operating condition.

coefficient increases with the increase in distance from the bottom to top, suggesting a predominantly downflowing solid layer next to the water wall surface, with fresh cold solids coming into contact with the top part of the surface.

Experiment shows that, heat transfer coefficients increase with an increase in the solids circulation rates. More interestingly, for the same operating conditions, it is observed that heat transfer is higher on the water wall than that on the wing wall at a given elevation (Case 2) shown in Fig. 12.

The difference in heat transfer coefficients between water wall and wing wall is lower when the wing wall was at the top of the riser (Case 1). As mentioned earlier, the hydrodynamic condition on the wing wall in Case 1 is similar to that on the water wall which is characterized by a net downward solids flux. When the wing wall is placed at mid-height (Case 2), the hydrodynamics condition is one of dispersed flow with net upward solid flux. However, the heat transfer coefficient in Case 2 is greater than the heat transfer coefficient without solids because of a flatter boundary layer over the wing wall and total absence of particle convection.

4. Conclusion

The experimental investigation on the wing wall for the bench scale laboratory unit shows the following:

1. The hydrodynamic condition on the wing wall is different from that on the water wall.
2. At any operating condition the heat transfer coefficient on the wing wall is lower than that on the water wall irrespective of its position.
3. The position of the wing wall affects both hydrodynamics and heat transfer. A wing wall placed at the top of the CFB riser has higher heat transfer coefficients than that when placed at the mid height of the CFB riser. This is due to a downward solids flow at the top corner of the riser.
4. No downward solids flow was noticed while the wing wall was placed at mid height.
5. While modeling heat transfer in a rectangular riser, the corner affect should be taken into consideration because of its influence on both hydrodynamics as well as heat transfer rates.

Acknowledgements

The authors acknowledge the financial supports from Natural Science and Engineering Research Council of Canada. We thank Canadian International Development Agency for allowing the use of CFB pilot plant. The authors also thank Michel Horne and Pete Langille for their assistance in conducting the tests.

References

[1] P. Basu, P.K. Nag, Heat transfer to walls of a circulating fluidized-bed furnace, Chem. Eng. sci. 51 (1) (1996) 1–26.

[2] L.R. Glicksman, Heat transfer in circulating fluidized beds, in: J.R. Grace, A.A. Avidan, T.M. Knowlton (Eds.), Circulating Fluidized Beds, Chapman & Hall, London, 1997, pp. 261–310.
[3] O. Molerus, K.-E. Writh, in: Heat Transfer in Fluidized Beds, first ed., Chapman & Hall, London, 1997, pp. 111–151.
[4] Claes Breitholtz, Heat transfer in circulating fluidized bed boilers, PhD thesis, Chalmers University of Technology, Goteborg, Sweden, 2000.
[5] P. Basu, P.K. Nag, An investigation into heat transfer in circulating fluidized beds, Int. J. Heat Mass Transfer 30 (11) (1987) 2399–2409.
[6] A. Mosyak, E. Pogrebnyak, G. Hetsroni, Effect of constant heat flux boundary condition on wall temperature fluctuations, J. Heat Transfer 123 (2) (2001) 213–218.
[7] M.J. Rhodes, P. Laussmann, F. Villain, D. Geldert, Measurement of radial and axial solids flux variations in the riser of a circulating fluidized bed, in: P. Basu, J.F. Large (Eds.), Proceedings of Second International Conference on Circulating Fluidized Beds, Compiegne, France, 1988, pp. 155–164.
[8] W. Zhang, Fluid dynamic of the transport zone of circulating fluidized beds with application to boiler, PhD thesis, Chalmers University of Technology, Goteborg, Sweden, 1995.
[9] J.C. Moran, L.R. Glicksman, Gas velocities and gas boundary layers inside a riser of a circulating fluidized bed, in: Donald W. Geiling (Ed.), Sixteenth FBC Conference on Fluidized Bed combustion, (FBC 01-0027) Reno, Nevada 2001.
[10] C.B. Rogers, J.K. Eaton, The behavior of solid particles in a vertical turbulent boundary layer in air, Int. J. Multiphase Flow 16 (5) (1990) 819–834.
[11] M. Rashidi, G. Hetsroni, S. Banarjee, Particle-turbulence interaction in a boundary layer, Int. J. Multiphase Flow 16 (5) (1990) 935–949.
[12] M. Hussainov, A. Kartushinsky, A. Mulgi, I. Shcheglov, S. Tisler, Experimental study of two-phase flow past various bodies and deposition of solid particles on the surfaces, Proceedings of Second Baltic Heat Transfer Conference, Jurmala, Latvia, August 21–23, 1995, Adv. Eng. Heat transfer pp. 267–276.
[13] R.L. Wu, J.R. Grace, C.J. Lim, C.M.H. Brereton, Suspension to surface heat transfer in a circulating fluidized bed combustor, AIChE J. 35 (10) (1989) 1685–1691.
[14] R.L. Wu, C.J. Lim, J. Chaouki, J.R. Grace, Heat transfer from a circulating fluidized bed to membrane waterwall surfaces, AIChE J. 33 (1987) 1888–1893.
[15] J. Zhou, J.R. Grace, S. Qin, C.M.H. Brereton, C.J. Lim, J. Zhu, Voidage profiles in a circulating fluidized bed of square cross-section, Chem. Eng. Sci. 49 (19) (1994) 3217–3226.
[16] W. Luan, C.J. Lim, C.M.H. Brereton, B.D. Bowen, J.R. Grace, Experimental and theoretical study of total and radiative heat transfer in circulating fluidized beds, Chem. Eng. Sci. 54 (1999) 3749–3764.